Diminished cortical excitation during perceptual impairments in a mouse model of autism

Joseph Del Rosario[1], Anderson Speed[1], Hayley Arrowood[1], Cara Motz[1,2], Machelle Pardue[1,2], Bilal Haider[1,*]

[1] Biomedical Engineering, Georgia Institute of Technology & Emory University, Atlanta, USA

[2] Atlanta VA Center for Visual and Neurocognitive Rehabilitation, Decatur, USA

*Lead contact: bilal.haider@bme.gatech.edu

Abstract

Sensory impairments are a core feature of autism spectrum disorder (ASD). These impairments affect visual perception, and have been hypothesized to arise from imbalances in excitatory and inhibitory activity in cortical circuits; however, there is little direct evidence testing this hypothesis with direct recordings of excitatory and inhibitory neural activity during relevant impairments of sensory perception. Here, we utilized a genetically relevant mouse model of ASD (CNTNAP2$^{-/-}$ knockout, KO) and recorded putative excitatory and inhibitory population spiking in primary visual cortex (V1) while measuring visual perceptual behavior. We found that KO mice showed quantitative impairments in both the speed and accuracy of visual perception. These impairments were simultaneously associated with diminished excitatory neuron activity and elevated low frequency network oscillations in superficial cortical layers 2/3 (L2/3). These results establish that perceptual deficits associated with ASD can arise from reduced sensory firing of excitatory rather than inhibitory neurons in cortical circuits.

Introduction

Impaired sensory perception is a key feature of autism spectrum disorder (ASD) (Robertson & Baron-Cohen, 2017). Sensory disturbances may occur in >90% of individuals with ASD (Tavassoli, Miller, Schoen, Nielsen, & Baron-Cohen, 2014), and are present early in development (Tomchek & Dunn, 2007). These sensory symptoms can predict later disease severity (Estes et al., 2015). Since there is detailed knowledge about the neural circuit basis of mammalian sensory processing, understanding impaired sensory perception in autism models provides an entry point for identifying neural circuit dysfunctions underlying core symptoms of ASD.

A prominent theory of ASD proposes that imbalanced excitatory-inhibitory activity ratios in cortex generate behavioral deficits (Nelson & Valakh, 2015; Rubenstein & Merzenich, 2003; Sohal & Rubenstein, 2019). However, little direct evidence for this hypothesis has been measured from identified excitatory and inhibitory neurons during quantifiable behavioral impairments. One recent study found that inhibitory neurons are more perturbed than excitatory neurons in superficial cortical layers 2/3 (L2/3) in a Fragile X syndrome mouse model of ASD (Goel et al., 2018). However, another study of ASD model mice observed reduced and poorly coordinated excitatory activity in frontal cortex of CNTNAP2$^{-/-}$ KO mice (Lazaro et al., 2019), but these excitatory activity deficits were not measured during sensory impairments or behavior. A third study suggests that these and multiple other

ASD models internally compensate for deficits of excitatory and inhibitory activity, resulting in overall preserved sensory responsiveness (Antoine, Langberg, Schnepel, & Feldman, 2019); crucially, this study also did not measure neural activity deficits during sensory perceptual impairments. It thus remains unresolved if excitatory or inhibitory neural activity deficits underlie simultaneous perceptual impairments in ASD mouse models.

There is extensive mechanistic knowledge about the excitatory and inhibitory basis of visual processing (Douglas & Martin, 2004; Isaacson & Scanziani, 2011; Priebe & Ferster, 2012), providing an ideal framework for resolving questions about neural activity deficits and perceptual impairments in ASD. Remarkably, deficits of visual processing arise as early as primary visual cortex (V1) in individuals with ASD (Robertson et al., 2014). We recently established that the state of cortical activity in V1 plays a decisive role for trial-by-trial visual spatial perception in mice (Speed, Del Rosario, Burgess, & Haider, 2019). This platform enabled us to record putative excitatory and inhibitory neuron spiking in V1 of a genetically relevant mouse model of ASD (CNTNAP2$^{-/-}$ Knockout, KO), while measuring the speed and accuracy of perceptual behavior. We found that KO mice showed quantitative deficits in visual perception, and these were associated with diminished excitatory neuron activity and aberrant low frequency network oscillations in the superficial layers of V1.

Results

We trained both C57BL6J (wildtype, WT) and CNTNAP2$^{-/-}$ knockout (KO) mice to report perception of spatially localized visual stimuli. Mice learned to lick for water rewards when visual stimuli (horizontally oriented Gabor gratings, see Methods) appeared on a screen (Fig. 1A). Stimuli appeared only after a mandatory period of no licking (0.5 – 6 s, randomized per trial), and rewards were delivered only upon the first lick during the stimulus response window (typically 1 – 1.5s in duration). We quantified perceptual performance using signal detection theory (Green & Swets, 1974). Our prior studies in WT mice showed that detection of stimuli in the peripheral (monocular) visual field is more difficult than detection in the central (binocular) visual field (Speed et al., 2019). Here we found that KO mice had lower detection sensitivity than WT mice for stimuli appearing in these more difficult (monocular) spatial locations. Spatial detection sensitivity dropped to chance level at significantly nearer eccentricity in KO versus WT mice (49 ± 4˚, n = 5 KO mice vs 72 ± 2˚, n = 7 WT mice, $p<0.01$ single tail rank sum). Since the goal of our study was to examine neural activity deficits in KO mice during repeatable and robust measurements of perceptual performance, here we focused on examining neural correlates of visual detection in the binocular visual field (central 20˚). This allowed us to measure large numbers of correct and incorrect behavioral trials, while presenting visual stimuli at the same spatial locations, visual contrasts, and durations for both WT and KO mice (see Methods).

KO mice detected binocular visual stimuli more slowly and less accurately than WT mice. KO mice showed significantly slower reaction times (Fig. 1B-C), and significantly fewer correct (Hit) trials of stimulus detection (Fig. 1D) than WT mice. However, KO mice also made fewer false alarms, which overall led to psychometric detection sensitivity (d') that did not differ significantly from WT mice (Fig. 1E-F, see Methods). These measurements also revealed that KO mice

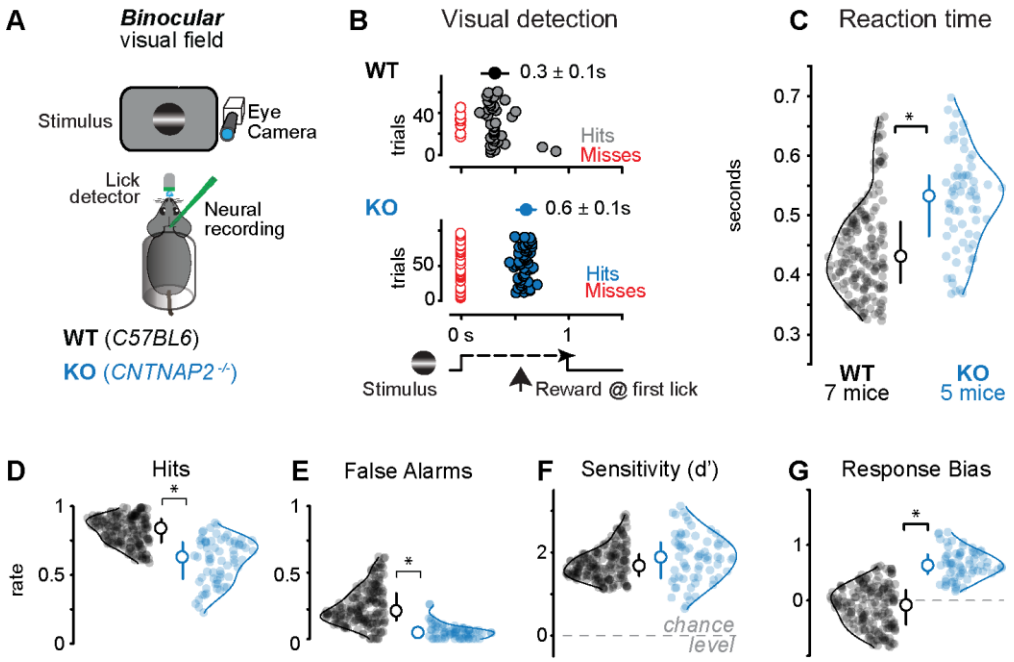

Figure 1. Visual perceptual behavior is impaired in the CNTNAP2$^{-/-}$ mouse model of ASD

- **A.** Head-fixed mice were trained to detect visual stimuli in the binocular visual field by licking to obtain water reward. Pupil activity, neural activity, and licking was recorded simultaneously with behavior. C57BL6J (Wildtype, WT) in black, CNTNAP2$^{-/-}$ (KO) in blue throughout.
- **B.** Example behavioral session shows detection latency (reaction time) was markedly slower for KO versus WT mice. Stimulus time course shown at bottom, with first lick times on correct trials (hits, colored circles) shown for individual consecutive trials (ordinate). Failures of detection (Misses) plotted in red. Average reaction times: WT, 0.3 ± 0.1s; KO, 0.6 ± 0.1s, mean ± SD reported throughout the figure.
- **C.** KO mice detected stimuli significantly more slowly than WT mice (KO: 0.52 ± 0.08, 71 sessions, 7 mice; WT: 0.45 ± 0.08, 187 sessions, 5 mice; $p < 0.01$). Average stimulus contrast was similar across KO and WT mice (WT: 23 ± 24%; KO: 23 ± 22%). Circles show reaction time average per session. Median ± IQR plotted inside the distributions.
- **D.** KO mice showed significantly lower hit rates (KO: 0.6 ± 0.18; WT: 0.82 ± 0.12; $p < 0.01$).
- **E.** KO mice showed significantly lower false alarm rates (KO: 0.06 ± 0.07; WT: 0.24 ± 0.15; $p < 0.01$).
- **F.** Sensitivity index (d') was not different between KO and WT mice (KO: 1.84 ± 0.71; WT: 1.74 ± 0.47; $p = 0.1$).
- **G.** KO mice showed higher criterion (c) indicating increased bias to withhold from responding (WT: 0.12 ± 0.43; KO: 0.65 ± 0.29; $p < 0.01$). Criterion was significantly greater than 0 for KO mice, but not for WT mice (WT: $p = 0.06$; KO: $p < 0.01$). C – G all during same behavioral trials.

held a significantly more conservative response bias than WTs (Fig. 1G). However, this conservative response bias was not simply explained by lower arousal—in fact, KO mice showed higher arousal (measured via pupil area) than WT mice before stimulus onset (Fig. 2D), and both WT and KO mice showed relatively lower arousal preceding correct detection, consistent with prior reports (McGinley et al., 2015; Speed et al., 2019). Higher arousal did not lead to higher distractibility in KO mice. We measured the rate of premature responses (stray licks) during pre-stimulus periods as a proxy of distraction (impulse control) in head-fixed mice performing lick response tasks (Fonseca, Murakami, & Mainen, 2015). We found that KO mice showed significantly

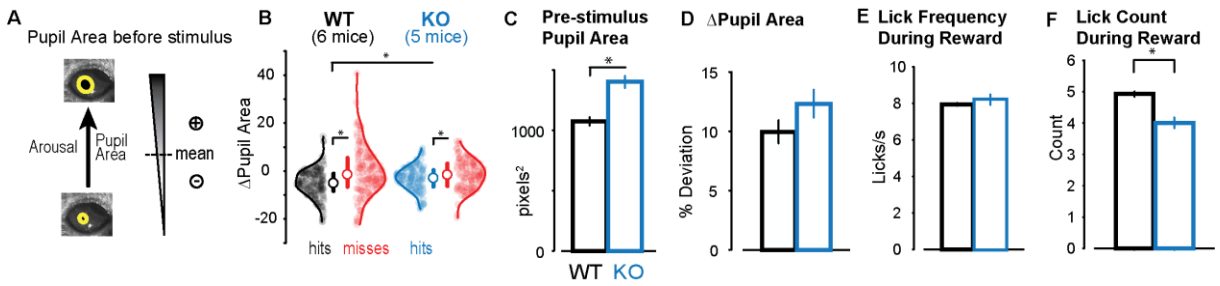

Figure 2. Arousal and motor activity do not explain perceptual impairments

- **A.** Pupil area was measured during each trial. Larger positive deviation of pupil area from mean indicates higher arousal.
- **B.** ΔPupil area preceding stimulus onset on Hit trials was significantly smaller than Miss trials in both WT (Hits: -5.2 ± 0.5%; Misses: -0.5 ± 0.8%; n = 190 sessions in 6 mice; mean ± SEM throughout the figure; *p<0.01*, rank sum test) and KO mice (Hits: -3.2 ± 0.5%; Misses: -1.5 ± 0.6%; n = 138 sessions in 5 mice; *p<0.01,* rank sum test). ΔPupil area preceding Hits was significantly smaller in WT versus KO mice (*p<0.01*, rank sum test), but not for Misses (*p=0.65*, rank sum test). ΔPupil area was calculated as the frame-by-frame percent deviation from the mean pupil area of the whole recording session (see Methods). Median ± IQR is plotted inside the distributions.
- **C.** Overall mean pupil area was larger in KO versus WT mice (WT: 1075 ± 35 pixels^2, KO = 1402 ± 51 pixels^2; *p<0.01,* rank sum test).
- **D.** ΔPupil area during reward consumption was not significantly different between WT (10.0 ± 1.0%) and KO mice (12.3 ± 1.2%; *p=0.57*, rank sum test).
- **E.** Lick frequency during reward was not significantly different between WT (8.0 ± 0.1) and KO mice (8.2 ± 0.3; *p=0.12,* rank sum test).
- **F.** Lick count during reward bouts was significantly smaller in KO mice (4.0 ± 0.2) compared to WT mice (5.0 ± 0.1, *p < 0.01*, rank sum test).

fewer premature responses than WT mice (KO: 1.41 ± 0.16 stray licks / trial; WT: 2.42 ± 0.11, *p < 0.01*); moreover, premature responses in KO mice were not significantly modulated by arousal (1.5 ± 0.1 stray licks / trial versus 1.6 ± 0.1, sorted relative to median pupil area, *p = 0.73,* rank sum test). This suggests that KO mice do not show greater distractibility as a function of arousal. Moreover, response vigor was comparable for KO and WT mice on Hit trials (similar licking frequencies, one fewer lick per reward in KO mice, Fig. 2E), arguing against gross motor deficits as a main factor for perceptual impairments.

We next measured visual neural responses, and found that KO mice displayed weaker excitatory sensory processing in V1, but only during wakefulness. We first measured fast spiking (FS, putative inhibitory) and regular spiking (RS, putative excitatory) neuron populations (Fig. 3A) with silicon probe recordings across layers of V1 during anesthesia; here we observed no differences in the overall distributions of visually-evoked spiking in either RS or FS neurons of KO versus WT mice (Fig. 4B, D). In contrast, recordings during wakefulness (in the absence of the behavioral task) revealed that visually-evoked spiking of RS neurons in KO mice was significantly reduced versus WTs, but with no differences in FS neuron responses during the same recordings (Fig. 4A, C).

Reduced responses in KO mice were not simply explained by lower baseline

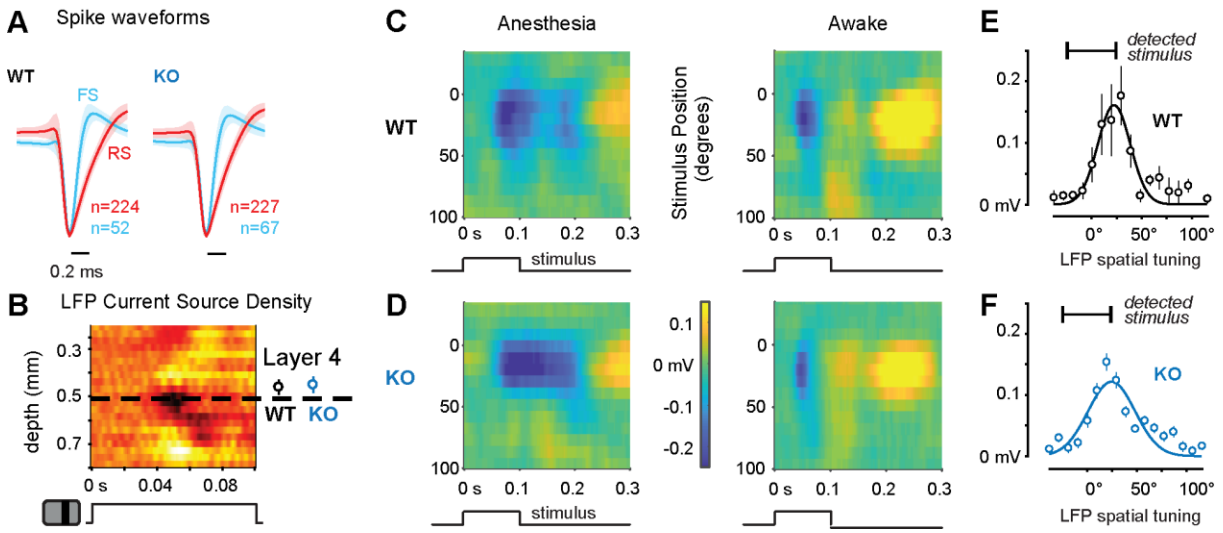

Figure 3. Cell types, laminar estimates, receptive fields, and stimulus positioning were similar across WT and KO recordings

- **A.** Population spike waveforms of fast-spiking (FS) putative inhibitory neurons and regular spiking (RS) putative excitatory neurons in WT and KO mice (mean ± SEM). Individual waveforms normalized to maximum negative deflection before averaging.
- **B.** Left, Example current source density (CSD) heatmap showing response to high contrast bar onset in best spatial location. Rows indicate LFP sampled across cortical layers, stimulus time course at bottom. Dark colors identify earliest and largest current sink, presumed to be layer 4 (L4). Right, population estimates of L4 from CSD are similar across WT (0.51 ± 0.02 mm, mean ± SEM, n = 23) and KO mice (0.51 ± 0.02 mm, n = 28).
- **C.** Spatial tuning of local field potential (LFP) responses in V1 of WT mice recorded during anesthesia (left; n = 13 recordings, 4 mice) and wakefulness (right; n = 10 recordings, 4 mice). Ordinate indicates stimulus (bar) position (in azimuth, vertical meridian at 0˚), abscissa shows time course. Note that both WT and KO spatial tuning peaks within the central 20˚ of the visual field, in the binocular zone.
- **D.** Same as c, for KO mice during anesthesia (left, n=18 recordings, 4 mice) or wakefulness (right, n = 10 recordings, 4 mice). Note that state-dependent amplitude and time course of LFP spatial tuning is similar across KO and WT recordings.
- **E.** Spatial tuning of population LFP response in awake WT mice (line shows Gaussian fit, peak at 22˚). The position and extent of stimuli detected during the task shown at top.
- **F.** Same as E, for KO mice. Gaussian fit peaks at 24˚. Receptive field size (half-width of peak-normalized Gaussian fit) was not significantly different between WT (18 ± 5˚, mean ± SD) and KO (15 ± 4˚) mice during anesthesia (*p=0.29,* rank sum test) or wakefulness (19 ± 14˚; 18 ± 9˚; *p=0.96,* rank sum test).

excitability, smaller receptive fields, or slower response latencies. First, baseline firing rates were not different in WT and KO mice (RS: WT = 2.55 ± 0.32, KO=2.96 ± 0.32, *p=0.39*; FS: WT = 6.16 ± 1.35, KO=6.53 ± 1.14, *p=0.43*, single-tail rank sum test). Second, receptive field properties (spatial extent and width) were comparable in WT and KO mice (Fig. 3E, F). Third, the amplitude and latency of LFP responses during wakefulness was in fact significantly faster in KO mice across all layers (Fig. 3 – Suppl. 1, L2/3: WT = 58 ± 42 ms, KO=50 ± 4 ms, *p=0.05*, rank sum test; L4: WT = 59 ± 4 ms, KO = 49 ± 1 ms, *p=0.01*, rank sum test; L5/6: WT = 59 ± 6 ms, KO = 49 ± 4 ms, *p<0.01*, rank sum test). Finally, perceptual impairments were not explainable by slower

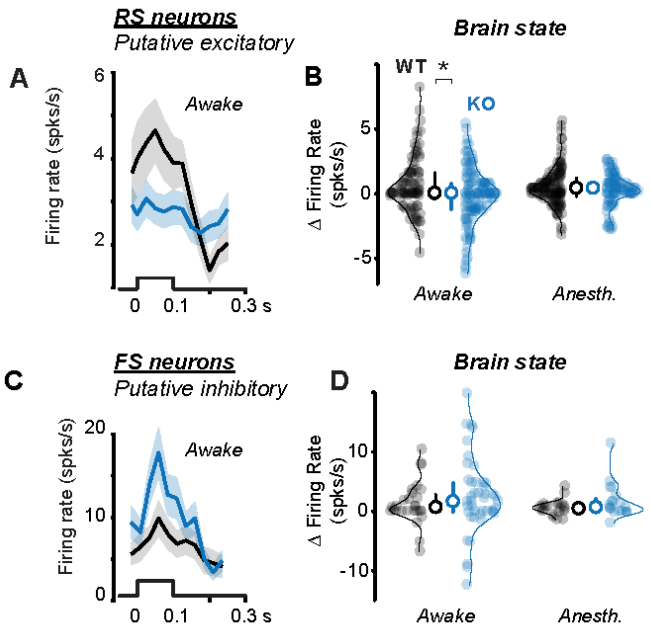

Figure 4. Reduction of visually-evoked RS neuron firing in KO mice depended on brain state

- **A.** Peristimulus time histograms (PSTHs) of awake visual responses (high contrast bars, bottom) in regular spiking (RS) putative excitatory neurons. Mean ± SEM.
- **B.** Left, responses in KO mice were significantly reduced during wakefulness (WT: Δ0.72 ± 0.33 spikes / s, n = 95 neurons; KO: Δ-0.22 ± 0.24, n = 131 neurons; *p<0.05*, single-tail rank sum test). Right, no significant difference during anesthesia (WT: Δ0.59 ± 0.17 spikes / s, mean ± SEM reported throughout figure, n = 129 neurons; KO: Δ0.24 ± 0.14, n = 96 neurons; *p=0.29*, single-tail rank sum test). Median and IQR plotted inside distributions. ΔResponse calculated as difference between pre- and post-stimulus activity (see Methods).
- **C.** Same as A, for fast spiking (FS) putative inhibitory neurons.
- **D.** No significant difference in fast spiking (FS) putative inhibitory neuron responses during wakefulness (WT: Δ1.61 ± 0.95 spikes / s; n = 45 neurons; KO: Δ2.44 ± 1.09, n = 29 neurons; *p=0.21,* single-tail rank sum test) or anesthesia (WT: Δ0.66 ± 0.33 spikes / s; n = 23 neurons; KO: Δ1.84 ± 0.84, n = 22 neurons; *p=0.55*, single-tail rank sum test).

or reduced visual responses in the retina—these were nearly identical in KO and WT mice across a wide range of light intensities (Fig. 1 – Suppl. 1).

Consistent with a specific deficit during wakefulness, KO mice also displayed reduced RS neuron activity during perceptual behavior. Recordings in binocular V1 (Fig. 3C-F) revealed fewer visually-evoked spikes in RS neurons of KO mice on correct binocular detection (Hit) trials (Fig. 5A-B). These activity deficits were not apparent on incorrect detection (Miss) trials and were not apparent in FS neurons (Fig. 5C-D). Again, these results were not explainable by slower neural response latencies: LFP response latencies to stimuli detected on Hit trials were not significantly different in WT versus KO mice (L2/3: WT=78 ± 4 ms, KO=75 ± 3 ms, *p=0.65;* L4: WT=78 ± 4 ms, KO=76 ± 3 ms; *p=0.8*; L5/6: WT=71 ± 3 ms, KO=70 ± 2 ms; *p=0.7)*. If anything, KO neural responses were slightly faster than WTs, consistent with prior findings (Bertone, Mottron, Jelenic, &

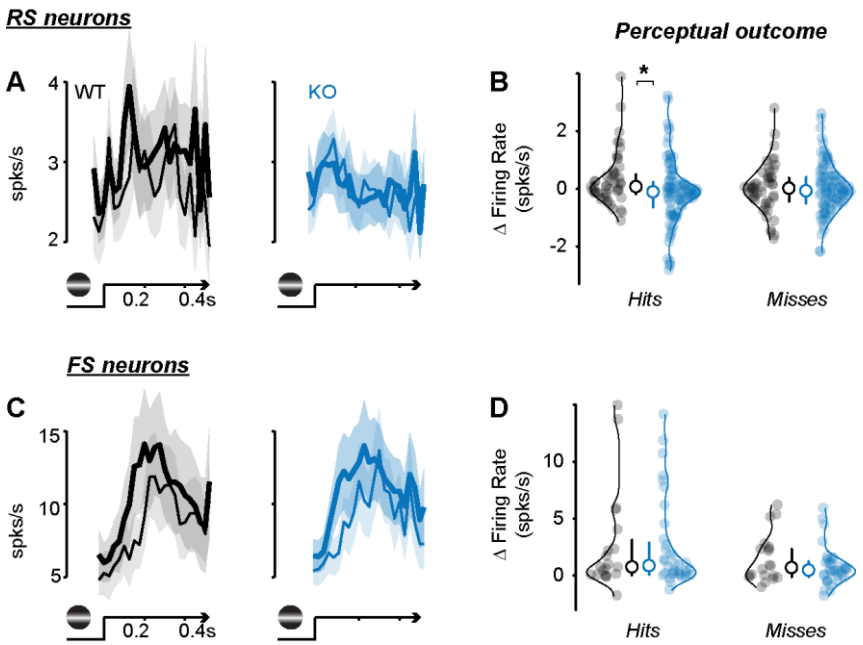

Figure 5. Diminished visual responses in RS neurons of KO mice depend upon perceptual outcome

- **A.** Peristimulus time histograms (PSTHs) of regular spiking (RS) putative excitatory neurons during correct detection trials (hits) in WT (left) and KO mice (right). Mean ± SEM. Thick lines indicate high contrast trials (WT: 28 ± 14%; ASD: 28 ± 13%, mean ± SD) while thin lines indicate low contrast trials (WT: 6 ± 4%; ASD: 5 ± 2%, mean ± SD).
- **B.** During perceptual behavior, RS activity was significantly reduced in KO mice selectively on correct detection (Hit) trials (WT: Δ0.45 ± 0.25 spikes / s, n = 49 neurons; KO: Δ–0.10 ± 0.14, n = 103 neurons; $p < 0.05$, single-tail rank sum test). Activity was not different during Miss trials (WT: Δ0.09 ± 0.1 spikes / s; KO: Δ0.02 ± 0.11, $p = 0.22$, single-tail rank sum test).
- **C.** Same as A, for fast spiking (FS) putative inhibitory neurons.
- **D.** No significant difference in FS activity on Hit trials (WT: Δ2.58 ± 0.10 spikes / s, n = 20 neurons; KO: Δ2.88 ± 0.84, n = 38 neurons; $p=0.78$, single-tail rank sum test) or Miss trials (WT: Δ1.40 ± 0.47 spikes / s; KO: Δ0.81 ± 0.34; $p=0.43$, single-tail rank sum test).

Faubert, 2005). Again, the deficits in RS neuron activity in KO mice were not due to increased arousal assessed via pupil dilation: increased arousal resulted in significantly higher (not lower) firing rates (Fig. 5 – Suppl. 1, r = 0.98, $p < 0.01$). We also examined trial-to-trial variability in both LFP and spiking responses, and this was also comparable in WT versus KO mice and did not explain behavioral differences (not shown here).

Deficits in excitatory neuron activity in KO mice were most pronounced in Layer 2/3 (L2/3). We identified cortical layers in V1 using current source density analysis (Fig. 3B), and assigned neural activity to L4, L2/3, and L5/6. Overall, activity levels were lower in L2/3 of KO mice during behavioral recordings (Fig. 6A), and we isolated fewer neurons in L2/3 of KO versus WT mice. We aggregated across all awake recordings (both inside and outside of the behavioral task) and found that L2/3 excitatory neurons in KO mice showed significantly smaller action potential waveforms versus WT mice (Fig. 6B). Consistent with these observations, we observed lower multi-unit

(MU) activity (not shown here) and lower peak-to-peak visually-evoked LFP amplitude specifically in L2/3 of KO versus WT mice (Fig. 6C). Importantly, in these same recordings, RS and FS neurons in L4 and L5/6 did not show significant differences in action potential amplitudes or activity profiles during behavior (L4: FS, $p=0.27$; RS, $p = 0.35$; L5/6: FS, $p=0.29$, RS, $p = 0.12$; rank sum tests), arguing against a global activity deficit in KO mice. Furthermore, the reduction in firing was not a consequence of increased arousal in KO mice, since firing rates in all layers increased as a function of pupil area (Fig. 5 – Suppl. 1).

We performed several control measures to assess if differences in L2/3 RS activity were due to experimental conditions in KO mice. First, background activity levels were comparable (or smaller) in recordings from KO versus WT mice, suggesting that reduced single-unit isolation in L2/3 was not because of higher unresolved background activity levels (Fig. 6 – Suppl. 1). Second, AP amplitudes were orders of magnitude larger than the background levels in both WT and KO recordings (Fig. 6 – Suppl. 1). Third, the overall percentage of L2/3 RS neurons within a recording was not significantly different in WT and KO mice (WT: 4.2 ± 3.0%, n = 15 recordings; KO: 0.5 ± 0.4%, n = 24 recordings; mean ± SEM, $p=0.13$, one-tail rank sum test). Fourth, the percentage of RS neurons isolated in other layers did not uniformly decrease in KO mice (L5/6 – WT: 61 ± 7%, KO: 83 ± 6%, $p<0.05$, one-tail rank sum test; L4 – WT: 35 ± 7%, KO: 17 ± 6%, $p<0.05$, one-tail rank sum test). Lastly, the majority of L2/3 RS neurons in both WT and KO mice were recorded across multiple consecutive recording sessions 24 – 48 hours after the initial craniotomy (WT, 66.7% of total; KO, 51% of total), suggesting that the quality and longevity of experimental preparations were comparable in WT and KO mice.

During perceptual behavior, L2/3 LFP in KO mice displayed aberrant low frequency power, and this degraded the relationship of neural activity to perceptual performance. We have recently shown that elevated low frequency (3 – 7 Hz) LFP power in V1 correlates with and predicts failures of stimulus detection in WT mice (Speed et al., 2019). Remarkably, in KO mice 3 – 7 Hz LFP power was significantly elevated on both correct and incorrect detection trials (Fig. 6D). Consequently, the difference in low frequency power on correct versus incorrect trials was less separable in KO mice (Fig. 6E). Consistent with our previous results, single-trial perceptual outcomes were accurately predicted from the 3 – 7 Hz LFP power in WT mice; however, perceptual outcome predictions from L2/3 LFP power were significantly worse in KO mice (Fig. 6F). Moreover, in WT mice L2/3 LFP power was significantly correlated with reaction time on correct trials (Fig. 6F, 48 ± 12% variance explained within mouse; 18 ± 1% variance explained across mice, $p < 0.05$); in contrast, L2/3 LFP power in KO mice was less predictive of reaction time (31 ± 8% within mouse; 3 ± 1% across mice, $p = 0.22$). These group differences were not captured by a single underlying relationship between LFP power and reaction times, since aggregating WT and KO data explained even less of the combined RT variance (<1%). Finally, elevated 3 – 7 Hz power in KO mice did not explain lower visually-evoked RS neuron firing rates (Fig. 5 – Suppl. 1). These results indicate that impairments in both the speed and accuracy of visual perception in KO mice are correlated with and predictable

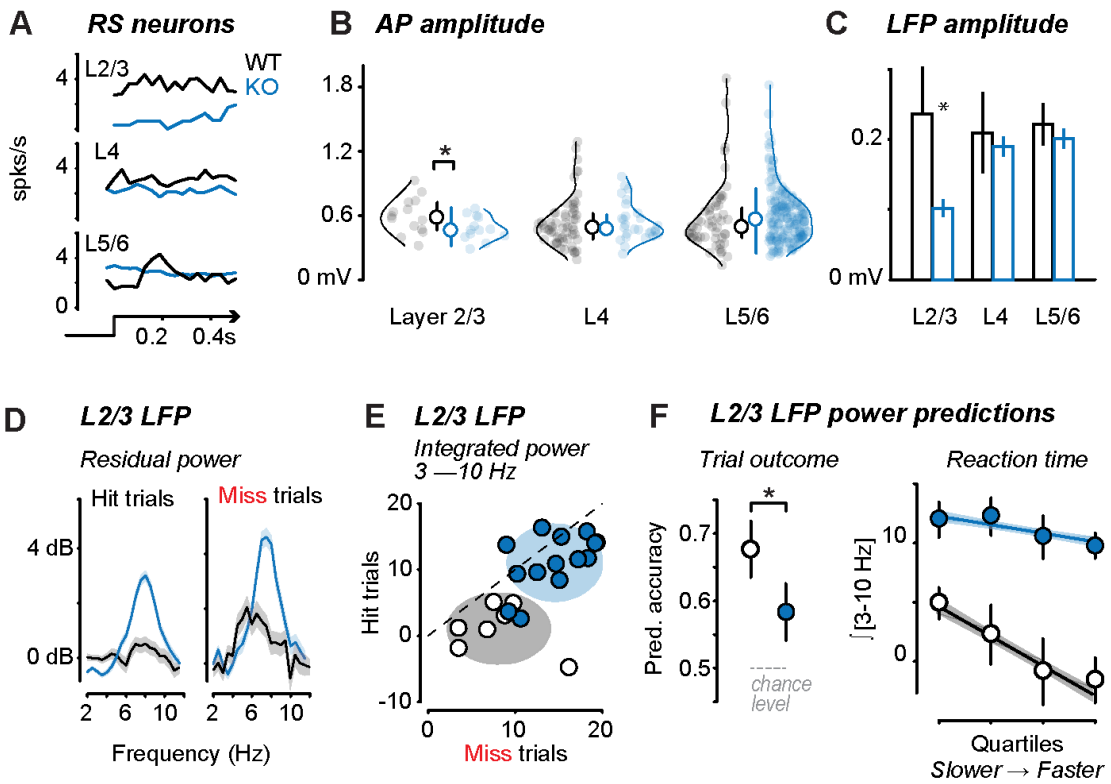

Figure 6. Aberrant neural activity in L2/3 correlates with perceptual impairments in KO mice

- **A.** Peristimulus time histograms (PSTHs) of average RS activity split by layers on correct detection trials.
- **B.** Action potential amplitudes in L2/3 RS neurons in KO mice were significantly smaller than in WT mice (0.48 ± 0.03 mV; mean ± SEM n = 13; 0.59 ± 0.04 mV, n = 14; *p<0.05*, single-tail rank sum test). There were no such differences in L4 (KO: 0.54 ± 0.03; n = 28; WT: 0.54 ± 0.03, n = 59; *p=0.35*) or L5/6 (KO: 0.59 ± 0.02; n = 178; WT: 0.58 ± 0.04, n = 53; *p=0.12)*. Neurons aggregated across anesthetized and awake recordings. Median ± IQR plotted inside distributions.
- **C.** Peak-to-peak stimulus-evoked LFP in L2/3 on Hit trials was significantly smaller in KO mice (98 ± 12 μV, mean ± SEM, n = 1402 trials, 15 recordings, 3 mice) versus WT mice (235 ± 68 μV, n = 533 trials, 7 recordings, 3 mice; *p<0.01*, single-tailed rank sum tests for all). No significant differences in other layers (L4: WT=207 ± 58μV, KO=189 ± 15μV, *p=0.31*; L5/6: WT=216 ± 30 μV, KO=190 ± 12 μV; *p=0.26*).
- **D.** Low frequency local field potential (LFP) residual power in L2/3 was significantly elevated in KO versus WT mice on both Hit trials (KO: 10.99 ± 0.65, n = 1402 trials, 15 recordings in 3 mice; WT: 1.21 ± 0.97, n = 533 trials, 7 recordings in 3 mice; *p<0.01*) and Miss trials (KO: 13.62 ± 0.98, n = 423 trials; WT: 7.33 ± 1.34, n = 211 trials; *p<0.01*). Mean ± SEM of integrated power 3 – 10 Hz. See Methods for calculation of residual power.
- **E.** Integrated 3-10Hz residual power was greater on Misses versus Hits in both KO and WT mice (*p<0.01* for both). Shaded regions show 2-D Gaussian fit (± 1σ).
- **F.** *Left,* Predictions of perceptual outcome from low frequency LFP power were significantly worse in KO mice (58 ± 4% accuracy; mean ± SD; cross-validated linear classifier) versus WT mice (68 ± 4% accuracy; *p<0.01*). See Methods for classifier description. *Right,* Low frequency LFP residual power was significantly and negatively correlated with reaction time in WT mice (r^2=0.18; *p<0.05*, F-test), but not in KO mice (r^2=0.03; *p=0.22*, F-test). Single trial reaction times (Hit trials) were binned into quartiles, and single trial integrated 3-10 Hz LFP residual power was averaged within quartile for all WT and KO trials (mean ± SEM). Shaded regions are bootstrap error of fits (see Methods).

from distinct excitatory neural activity deficits in L2/3.

Discussion

Here we showed that diminished excitatory signaling in cortex accompanies impaired sensory perception in the human-relevant CNTNAP2$^{-/-}$ mouse model of autism spectrum disorder (ASD). Using a well-controlled, head-fixed visual detection task, we quantified perceptual performance while recording V1 neural activity driven by spatially localized sensory stimuli. KO mice detected visual stimuli more slowly than WT mice and displayed simultaneous deficits of excitatory activity in L2/3. Population activity in L2/3 of KO mice was strongly synchronized at low frequencies (3 – 7 Hz) across all trial types. This aberrant low frequency activity was detrimental for predicting perceptual performance from neural activity in V1. Together, our results identify that excitatory rather than inhibitory activity deficits may underlie perceptual impairments in a genetically relevant mouse model of ASD.

Perceptual impairments in KO mice manifested as both slower and less accurate detection. The latency for generating rewarded motor actions was slower in KO versus WT mice, despite stimuli appearing at the same locations and same visual contrast ranges across experiments. Recent studies of visual perception using detection tasks have shown that both changes in sensitivity and response criterion contribute to perceptual performance, and that these two components of perception are dissociable with appropriate tasks and likely driven by distinct brain structures (Luo & Maunsell, 2018). Our results here in KO mice identify elevation of response criterion – the internal threshold to report detection— as one key component of behavioral impairments in KO mice. This elevated threshold for detecting stimuli occurs simultaneously with degraded visual responses in feedforward layers of V1. This suggests that in KO mice, brain areas representing the internal decision variable may receive degraded sensory information from V1, contributing to slower and less frequent detection of visual stimuli.

The latency of neural signals transmitted from V1 could not explain slower perception. In fact, response latencies in L4 of V1 were nearly identical in KO versus WT mice. Although individuals with ASD can also show slower and less reliable perceptual reaction times (Karalunas, Geurts, Konrad, Bender, & Nigg, 2014), this remains debated (Ferraro, 2016; van der Geest, Kemner, Camfferman, Verbaten, & van Engeland, 2001), and visual acuity and basic neuronal response latencies in individuals with ASD appear largely unaffected (Sutherland & Crewther, 2010; Tavassoli, Latham, Bach, Dakin, & Baron-Cohen, 2011). In our study, behavioral impairments were associated with and predicted by deficits in L2/3 RS neuron activity, the major source of feedforward projections to higher visual areas (Glickfeld, Andermann, Bonin, & Reid, 2013). One possibility is that feedforward visual signals of poorer quality are integrated more slowly in downstream areas in KO mice. Simultaneous recordings in V1, higher visual areas, and lick-related motor areas may reveal how deficits in the amplitude and timing of sensory-motor signals lead to delayed and impaired perception.

Perceptual impairments in KO mice were accompanied by several activity deficits in L2/3 excitatory neurons. First, sensory-evoked excitatory firing rates were significantly lower in a manner that depended upon brain state and behavioral

outcome. Second, action potential amplitudes in L2/3 RS neurons of KO mice were significantly smaller than in WT mice. Third, perceptual impairments in KO mice were accompanied by elevated low frequency power in L2/3. These specific deficits in L2/3 cortical excitatory neurons dovetail with recent findings in humans revealing that individuals with ASD show specific alterations in L2/3 cortical excitatory neurons (Velmeshev et al., 2019). We discuss each of these deficits in greater detail below.

Excitatory neural activity deficits in KO mice were dependent upon brain state. Recordings of both FS inhibitory and RS excitatory neurons during anesthesia did not reveal overall differences in visually-evoked firing rates; however, recordings during wakefulness revealed reduced responses in RS excitatory neurons specific to behavioral conditions, cortical layers, and perceptual outcomes. This suggests that the effects of anesthesia (Haider, Hausser, & Carandini, 2013) may mask identification of fine-scale cortical neural activity deficits in mouse models of ASD. Lower excitatory firing was apparent even though mice detected low contrast, static stimuli that drove neural activity far less vigorously than drifting, high-contrast stimuli typical of many studies of mouse V1 (Durand et al., 2016; Michaiel, Parker, & Niell, 2019). This highlights the need to not only compare neural circuit deficits across multiple mouse models of ASD (Antoine et al., 2019), but to also compare across multiple brain states, stimulus sets, and behavioral outcomes. Although we found that differences in arousal could not explain perceptual impairments, neural activity deficits may be more pronounced with behaviorally relevant engagement of neuromodulatory systems, an important topic for future investigations.

Smaller AP amplitudes in L2/3 RS neurons of KO mice may result from loss of CNTNAP2. A recent study of CNTNAP2$^{-/-}$ mice showed that loss of CNTNAP2 (a transmembrane protein) led to alterations in axonal K^+ channel localization, deficits in action potential waveforms, and reduced spontaneous synaptic activity in cortical L2/3 pyramidal neurons *in vitro* (Scott et al., 2019). These alterations could underlie the activity reductions, smaller extracellular action potentials, and reduced sensory responses measured here during perceptual behavioral impairments. Recordings of intracellular synaptic and action potentials in L2/3 neurons of awake KO mice could reveal greater insight about the mechanisms underlying these effects.

Several studies have revealed that increased 3 – 7 Hz LFP power impairs visual detection. We previously showed in WT mice that nearly 85% of perceptual failures were predicted by elevated 3 - 7 Hz LFP power (Speed et al., 2019), consistent with the detrimental role of these oscillations for visual coding in L2/3 (Einstein, Polack, Tran, & Golshani, 2017). Here, we found that KO mice showed significantly elevated low frequency power across all behavioral trials; this worsened the predictability of behavioral outcome from LFP activity and also obscured the relationship of LFP activity to reaction times on correct trials. It remains to be seen if low frequency oscillations play a causal role in directly impairing visual perception in KO mice, or if they are a network-wide consequence of reduced activity in specific excitatory neurons. One recent study directly induced low-frequency oscillations in primate visual cortex, and these caused visual

perceptual impairments (Nandy, Nassi, Jadi, & Reynolds, 2019). An intriguing possibility is that low frequency oscillations in L2/3 reduce the dynamic range available to transmit feedforward sensory information to downstream areas during behavior. This suggests that directly attenuating low frequency synchronization in L2/3 neurons may restore excitatory signaling bandwidth and remedy perceptual deficits, a hypothesis that now seems testable in mouse models.

Methods

Experimental model and subjects

All procedures were approved by the Institutional Animal Care and Use Committee at the Georgia Institute of Technology and were in agreement with guidelines established by the National Institutes of Health.

Surgery. Male C57BL6J (RRID: IMSR_JAX:000664) and CNTNAP2$^{-/-}$ (RRID: IMSR_JAX:017482) mice (5 – 8 weeks old; reverse light cycle individual housing; bred in house) were chronically implanted with a stainless steel headplate with a recording chamber during isoflurane (1-2%) anesthesia. The headplate was affixed to the skull using thin layer of veterinary glue (Vetbond) and secured using dental cement (Metabond). The recording chamber was sealed with a removable polymer (KwikCast). After implant surgery mice were allowed to recover for 3 days before experimentation. During recovery mice were habituated to experimenter handling.

Behavior

Water restriction. Following recovery from surgery, mice were placed under a restricted water schedule (to provide motivation) and trained to detect visual stimuli for water reward. Mice received a daily minimum amount of water (40 ml/kg/day; (Burgess et al., 2017; Speed et al., 2019). If mice did not receive their daily minimum water in task, they received supplemental hydration (Hydrogel).

Training. Mice first learned to associate visual stimuli with water reward through passive instrumental conditioning. For naïve mice to learn this association, water reward was delivered 0.7s after the onset of a visual stimulus (See “Visual stimuli”, below). Following reward consumption, mice then had to withhold from licking for a mandatory period of time (exponentially distributed intervals from 0.5-6s, randomly selected per trial) in order for visual stimuli to appear on subsequent trials. Lick times were measured with custom built contactless lick detectors (Williams, Speed, & Haider, 2018). Typically within 3 – 7 days of training, mice began licking shortly after stimulus onset and prior to reward delivery (anticipatory licking), indicating behavioral responses to the onset of the visual stimulus. Mice were then transitioned to an active paradigm where they only received rewards contingent upon licking during the stimulus presentation (typically 1 s long). On 20% of trials, 0% contrast stimuli were presented in order to measure the probability of licking to the absence of visual stimuli (false alarms). When detection performance was above chance for 2 consecutive days, the contrast and/or size of stimuli were decreased to maintain task difficulty. The main conclusions of this study involve detection of stimuli at a single position in the binocular visual field. Once performance was above chance for a range of low and high contrasts on binocular trials (2 - 33% contrast), we performed acute extracellular recordings.

Behavioral metrics. Detection performance was quantified with the psychometric

sensitivity index (d', (Green & Swets, 1974), which was calculated as:

$$d' = Z(hit\ rate) - Z(false\ alarm\ rate)$$

where Z represents the inverse of the normal cumulative distribution (MATLAB function norminv). Response bias or criterion (c) was calculated using the formula:

$$c = -\frac{Z(hit\ rate)+Z(false\ alarm\ rate)}{2}.$$

Higher criterion indicates more conservative response bias (withholding responses).

Recordings

Surgical preparation. A small craniotomy (100-400 microns) was opened over binocular V1 during isoflurane anesthesia. Mice were allowed ≥3 hours of recovery before awake acute recordings. There was no difference in behavioral performance in WT mice during recordings (d': 1.7 ± 0.5) versus the previous day (1.7 ± 0.2, $p = 0.6$, signed rank test). To remove any potential effect of anesthesia or surgery on perceptual performance in KO mice, craniotomies were performed 12-24 hours prior to recordings to ensure equally robust behavioral performance during recordings (d': 1.7 ± 0.2 versus 1.5 ± 0.3, $p = 0.4$). For anesthetized recordings, both KO and WT mice were given a combination of sedative chlorprothixene (0.1 mg/kg) and isoflurane (0.5-1%), as in our previous studies (Haider, Schulz, Hausser, & Carandini, 2016).

Electrophysiology. Single shank linear 32 site silicon probes (Neuronexus, A1x32) were used to record neural activity across cortical layers. The electrode was typically advanced to 1000 microns below the dura, and the site was covered in sterile artificial cerebrospinal fluid (aCSF). Recordings typically lasted 90 minutes, whereupon the probe was removed and the site cleaned with sterile aCSF and covered with polymer (Kwikcast). Typically we were able to record 3 consecutive days from the same craniotomy.

Visual stimuli. During behavior, mice detected Gabor gratings (0.05 - 0.1 cycles/°, σ = 10 - 20°, horizontal orientation, phase randomized per trial). Low contrast (5%) task-irrelevant bars (9˚ wide, 0.1s duration, inter-stimulus interval of 0.3s, vertical orientation) were also presented during the inter-trial intervals to facilitate receptive field mapping; these faint bars did not affect behavioral performance and they are not analyzed here. After task completion, 100% contrast bars (9˚ wide, 0.1s duration, inter-stimulus interval of 0.3s, vertical orientation, 100% contrast) were presented across the visual field to map the receptive field. These same bars were used to measure visual responses in awake mice not performing the behavioral task, and also during anesthetized experiments. The bar at the center of the receptive field and the adjacent ±1 bars were used in all subsequent analyses.

Eye Tracking. We recorded the animal's pupil during awake recordings. A high-speed camera (Imaging source DMK 21Bu04.H) with a zoom lens (Navitar 7000) and infrared filter (Mightex, 092/52x0.75) was placed ~22 cm from the animal's right eye. A near-infrared LED (Mightex, SLS-02008-A) illuminated the eye. Video files were acquired and processed using the Image Acquisition Toolbox in MATLAB with custom code. 1 mm corresponded to ~74 pixels on each frame.

Electroretinography. We tested retinal function using full-field flash electroretinography (ERG) as previously described (Mees et al., 2019). Briefly, after overnight dark-adaptation, we anesthetized mice (ketamine 60 mg/kg/, xylazine 7.5 mg/kg) under dim red light, anesthetized

corneas with tetracaine (0.5%; Alcon) and dilated pupils with tropicamide (1%; Sandoz). Binocular retinal responses were measured via gold-loop corneal electrodes, with platinum needle electrodes serving as reference and ground in the cheeks and tail, respectively. Testing consisted of 6 scotopic flashes (-4.86 – 2.5 log cd*s/m^2), followed by 10 minutes of light adaption (30 cd/m^2) and 3 photopic flashes (-0.2 – 1.4 log cd*s/m^2). Responses were differentially amplified (1-1500 Hz, 250 ms, 2 kHz) and stored (UTAS BigShot). We measured amplitude and implicit time for a and b waves (Penn & Hagins, 1969) and averaged the traces from right and left eyes for statistical analysis.

Analysis

Spike sorting. Electrical signals were acquired through a Cereplex Direct (Blackrock Microsystems). Raw neural signals were acquired at 30 kHz, and single unit activity was isolated with a semi-automated sorting algorithm (Rossant et al., 2016), as detailed in our previous studies (Speed et al., 2019). We classified single units as fast-spiking (FS, waveform peak-to-trough < 0.57ms) and regular spiking (RS, peak-to-trough > 0.57 ms) based on their waveform widths (Fig. 3A). FS neurons in mice are predominantly parvalbumin (PV) positive inhibitory neurons, while >85% of RS neurons are putative excitatory neurons (Pfeffer, Xue, He, Huang, & Scanziani, 2013; Speed et al., 2019).

LFP analysis. Local field potentials were band pass filtered at 0.3-200Hz. Layers were identified via current source density analysis (Niell & Stryker, 2008; Speed et al., 2019) and laminar LFP responses were calculated by taking the average across channels spanning particular layers. We analyzed the residual LFP power in hit and miss trials in the low frequency band (2-20 Hz). We calculated the residual LFP power by fitting the entire power spectrum with a single exponential that excluded the bandwidth of interest. In this bandwidth, residual LFP power is the difference between the measured power and power of the fit, normalized by the fit (Saleem et al., 2017; Speed et al., 2019).

LFP-behavior correlations. Reaction times was split into quartiles within each recording. The average residual power or stimulus-evoked spiking activity was then averaged for each quartile. A linear regression model was then fit to the data to determine if there was a correlation between neural activity and reaction time. Error bars were obtained by bootstrap resampling and repeating the fitting procedure 50 times.

Classifier. A support vector machine (SVM) classifier was constructed to predict trial outcome based on low frequency residual LFP power, as detailed elsewhere (Speed et al., 2019). The classifier was trained by randomly selecting 100 trials, and then a randomly sampled 100 trial test set was used to predict behavioral outcome (WT: hit trials = 533, miss trials = 211; KO: hit trials=1402, miss trials = 423). This procedure was repeated 50 times to obtain error bars (±SD) for classification accuracy.

Pupil analysis. Raw video frames were cropped to isolate the eye and pupil. Frames were smoothed with a 2-D Gaussian filter. Based on pixel intensity, the pupil was identified and a least-squares error 2D ellipse was fit to the contours. The pupil area was determined by the amount of pixels in the ellipse. ∆Pupil area was calculated as the percent deviation from the mean

$$\Delta \text{ Pupil area} = [\frac{(A-\bar{A})*100}{\bar{A}}],$$

where A is the area in pixels and $\bar{A}$ is the average area across all frames. Similarly, the

change in pupil position (azimuth) was calculated by subtracting the average position across all frames.

Stimulus-evoked analysis. Visually-evoked firing rates were calculated as the difference between pre-stimulus activity (0.1 s preceding the stimulus onset) and post-stimulus activity (anesthetized: 0 – 0.25 s; awake, no task: 0 – 0.125 s; awake, grating responses during task: 0 – 0.2 s). These windows were chosen based upon the duration of the LFP responses in each condition (Fig. 3C-D). This window thus captures both net increases and net decreases in firing rate induced by the visual stimulus, since many individual neurons experienced suppression of firing rates below baseline following the initial onset transient. This explains the large spread of positive and negative net firing rate changes evoked by the stimulus. Violin plots of individual data points in all figures show 95% of the data range (±2.5% of range clipped for display). All statistics used full data ranges.

Experimental design and statistical analysis

Our experimental design centered on measuring neural activity and behavior during identical sensory conditions, and comparing these across KO and WT mice matched in age, sex, recording region, and methods. Experimenters were not blinded to the group identity of each subject, but this was not required for performing identical measurements of behavioral performance or electrophysiology. We performed these studies in comparable numbers of subjects and experiments across groups. Throughout this paper, unpaired comparisons utilized Wilcoxon rank sum tests (tails specified) or sign tests (for differences from scalar values), and paired comparisons utilized Wilcoxon signed rank tests, unless otherwise noted.

Data availability

All data structures and code that generated each figure are available upon reasonable request.

Author contributions

J.D.R., H.A., A.S. performed behavioral experiments; J.D.R., A.S. performed electrophysiological experiments; C.M. performed ERG experiments and data analysis with M.P.; J.D.R., A.S., B.H. performed data analysis; J.D.R. and B.H. wrote the manuscript with feedback from all authors.

Acknowledgements

J.D.R. was funded by a Goizueta Foundation fellowship and Alfred P. Sloan Foundation's Minority Ph.D. (MPHD) Program Fellowship. B.H. was funded by the GT Neural Engineering center (1241384), the Whitehall Foundation, the Sloan Foundation, NIH NINDS (NS107968), NIH BRAIN Initiative (NS109978), and the Simons Foundation Autism Research Initiative (SFARI). M.P. was funded by Department of Veterans Affairs Rehabilitation Research and Development Service Merit Award (I01RX002615) and Senior Research Career Scientist Award (IK6RX003134).

References

Antoine, M. W., Langberg, T., Schnepel, P., & Feldman, D. E. (2019). Increased Excitation-Inhibition Ratio Stabilizes Synapse and Circuit Excitability in Four Autism Mouse Models. *Neuron, 101*(4), 648-661 e644. doi:10.1016/j.neuron.2018.12.026

Bertone, A., Mottron, L., Jelenic, P., & Faubert, J. (2005). Enhanced and diminished visuo-spatial information processing in autism depends on stimulus complexity. *Brain, 128*(Pt 10), 2430-2441. doi:10.1093/brain/awh561

Burgess, C. P., Lak, A., Steinmetz, N. A., Zatka-Haas, P., Bai Reddy, C., Jacobs, E. A. K., . . . Carandini, M. (2017). High-Yield Methods for Accurate Two-Alternative Visual Psychophysics in Head-Fixed Mice. *Cell Rep, 20*(10), 2513-2524. doi:10.1016/j.celrep.2017.08.047

Douglas, R. J., & Martin, K. A. (2004). Neuronal circuits of the neocortex. *Annu Rev Neurosci, 27*, 419-451. doi:10.1146/annurev.neuro.27.070203.144152

Durand, S., Iyer, R., Mizuseki, K., de Vries, S., Mihalas, S., & Reid, R. C. (2016). A Comparison of Visual Response Properties in the Lateral Geniculate Nucleus and Primary Visual Cortex of Awake and Anesthetized Mice. *J Neurosci, 36*(48), 12144-12156. doi:10.1523/JNEUROSCI.1741-16.2016

Einstein, M. C., Polack, P. O., Tran, D. T., & Golshani, P. (2017). Visually Evoked 3-5 Hz Membrane Potential Oscillations Reduce the Responsiveness of Visual Cortex Neurons in Awake Behaving Mice. *J Neurosci, 37*(20), 5084-5098. doi:10.1523/JNEUROSCI.3868-16.2017

Estes, A., Zwaigenbaum, L., Gu, H., St John, T., Paterson, S., Elison, J. T., . . . network, I. (2015). Behavioral, cognitive, and adaptive development in infants with autism spectrum disorder in the first 2 years of life. *J Neurodev Disord, 7*(1), 24. doi:10.1186/s11689-015-9117-6

Ferraro, F. R. (2016). No evidence of reaction time slowing in autism spectrum disorder. *Autism, 20*(1), 116-122. doi:10.1177/1362361314559986

Fonseca, M. S., Murakami, M., & Mainen, Z. F. (2015). Activation of dorsal raphe serotonergic neurons promotes waiting but is not reinforcing. *Curr Biol, 25*(3), 306-315. doi:10.1016/j.cub.2014.12.002

Glickfeld, L. L., Andermann, M. L., Bonin, V., & Reid, R. C. (2013). Cortico-cortical projections in mouse visual cortex are functionally target specific. *Nat Neurosci, 16*(2), 219-226. doi:10.1038/nn.3300

Goel, A., Cantu, D. A., Guilfoyle, J., Chaudhari, G. R., Newadkar, A., Todisco, B., . . . Portera-Cailliau, C. (2018). Impaired perceptual learning in a mouse model of Fragile X syndrome is mediated by parvalbumin neuron dysfunction and is reversible. *Nat Neurosci, 21*(10), 1404-1411. doi:10.1038/s41593-018-0231-0

Green, D. M., & Swets, J. A. (1974). *Signal detection theory and psychophysics*. Huntington, N.Y.,: R. E. Krieger Pub. Co.

Haider, B., Hausser, M., & Carandini, M. (2013). Inhibition dominates sensory responses in the awake cortex. *Nature, 493*(7430), 97-+. doi:Doi 10.1038/Nature11665

Haider, B., Schulz, D. P., Hausser, M., & Carandini, M. (2016). Millisecond Coupling of Local Field Potentials to Synaptic Currents in the Awake Visual Cortex. *Neuron, 90*(1), 35-42. doi:10.1016/j.neuron.2016.02.034

Isaacson, J. S., & Scanziani, M. (2011). How inhibition shapes cortical activity. *Neuron, 72*(2), 231-243. doi:10.1016/j.neuron.2011.09.027

Karalunas, S. L., Geurts, H. M., Konrad, K., Bender, S., & Nigg, J. T. (2014). Annual research review: Reaction time variability in ADHD and autism spectrum disorders: measurement and mechanisms of a proposed trans-diagnostic phenotype. *J Child Psychol Psychiatry, 55*(6), 685-710. doi:10.1111/jcpp.12217

Lazaro, M. T., Taxidis, J., Shuman, T., Bachmutsky, I., Ikrar, T., Santos, R., . . . Golshani, P. (2019). Reduced Prefrontal Synaptic Connectivity and Disturbed Oscillatory Population Dynamics in the CNTNAP2 Model of Autism. *Cell Rep, 27*(9), 2567-2578 e2566. doi:10.1016/j.celrep.2019.05.006

Luo, T. Z., & Maunsell, J. H. R. (2018). Attentional Changes in Either Criterion or Sensitivity Are Associated with Robust Modulations in Lateral Prefrontal Cortex. *Neuron, 97*(6), 1382-1393 e1387. doi:10.1016/j.neuron.2018.02.007

McGinley, M. J., Vinck, M., Reimer, J., Batista-Brito, R., Zagha, E., Cadwell, C. R., . . . McCormick, D. A. (2015). Waking State: Rapid Variations Modulate Neural and Behavioral Responses. *Neuron, 87*(6), 1143-1161. doi:10.1016/j.neuron.2015.09.012

Mees, L. M., Coulter, M. M., Chrenek, M. A., Motz, C. T., Landis, E. G., Boatright, J. H., & Pardue, M. T. (2019). Low-Intensity Exercise in Mice Is Sufficient to Protect Retinal Function During Light-Induced Retinal Degeneration. *Invest Ophthalmol Vis Sci, 60*(5), 1328-1335. doi:10.1167/iovs.18-25883

Michaiel, A. M., Parker, P. R. L., & Niell, C. M. (2019). A Hallucinogenic Serotonin-2A Receptor Agonist Reduces Visual Response Gain and Alters Temporal Dynamics in Mouse V1. *Cell Rep, 26*(13), 3475-3483 e3474. doi:10.1016/j.celrep.2019.02.104

Nandy, A., Nassi, J. J., Jadi, M. P., & Reynolds, J. (2019). Optogenetically induced low-frequency correlations impair perception. *Elife, 8*. doi:10.7554/eLife.35123

Nelson, S. B., & Valakh, V. (2015). Excitatory/Inhibitory Balance and Circuit Homeostasis in Autism Spectrum Disorders. *Neuron, 87*(4), 684-698. doi:10.1016/j.neuron.2015.07.033

Niell, C. M., & Stryker, M. P. (2008). Highly selective receptive fields in mouse visual cortex. *J Neurosci, 28*(30), 7520-7536. doi:10.1523/JNEUROSCI.0623-08.2008

Penn, R. D., & Hagins, W. A. (1969). Signal transmission along retinal rods and the origin of the electroretinographic a-wave. *Nature, 223*(5202), 201-204.

Pfeffer, C. K., Xue, M., He, M., Huang, Z. J., & Scanziani, M. (2013). Inhibition of inhibition in visual cortex: the logic of connections between molecularly distinct interneurons. *Nat Neurosci, 16*(8), 1068-1076. doi:10.1038/nn.3446

Priebe, N. J., & Ferster, D. (2012). Mechanisms of neuronal computation in mammalian visual cortex. *Neuron, 75*(2), 194-208. doi:10.1016/j.neuron.2012.06.011

Robertson, C. E., & Baron-Cohen, S. (2017). Sensory perception in autism. *Nat Rev Neurosci, 18*(11), 671-684. doi:10.1038/nrn.2017.112

Robertson, C. E., Thomas, C., Kravitz, D. J., Wallace, G. L., Baron-Cohen, S., Martin, A., & Baker, C. I. (2014). Global motion perception deficits in autism are reflected as early as primary visual cortex. *Brain, 137*(Pt 9), 2588-2599. doi:10.1093/brain/awu189

Rossant, C., Kadir, S. N., Goodman, D. F., Schulman, J., Hunter, M. L., Saleem, A. B., . . . Harris, K. D. (2016). Spike sorting for large, dense electrode arrays. *Nat Neurosci, 19*(4), 634-641. doi:10.1038/nn.4268

Rubenstein, J. L., & Merzenich, M. M. (2003). Model of autism: increased ratio of excitation/inhibition in key neural systems. *Genes Brain Behav, 2*(5), 255-267.

Saleem, A. B., Lien, A. D., Krumin, M., Haider, B., Roson, M. R., Ayaz, A., . . . Harris, K. D. (2017). Subcortical Source and Modulation of the Narrowband Gamma Oscillation in Mouse Visual Cortex. *Neuron, 93*(2), 315-322. doi:10.1016/j.neuron.2016.12.028

Scott, R., Sanchez-Aguilera, A., van Elst, K., Lim, L., Dehorter, N., Bae, S. E., . . . Marin, O. (2019). Loss of Cntnap2 Causes Axonal Excitability Deficits, Developmental Delay in Cortical Myelination, and Abnormal Stereotyped Motor Behavior. *Cereb Cortex, 29*(2), 586-597. doi:10.1093/cercor/bhx341

Sohal, V. S., & Rubenstein, J. L. R. (2019). Excitation-inhibition balance as a framework for investigating mechanisms in neuropsychiatric disorders. *Mol Psychiatry*. doi:10.1038/s41380-019-0426-0

Speed, A., Del Rosario, J., Burgess, C. P., & Haider, B. (2019). Cortical State Fluctuations across Layers of V1 during Visual Spatial Perception. *Cell Rep, 26*(11), 2868-2874 e2863. doi:10.1016/j.celrep.2019.02.045

Sutherland, A., & Crewther, D. P. (2010). Magnocellular visual evoked potential delay with high autism spectrum quotient yields a neural mechanism for altered perception. *Brain, 133*(Pt 7), 2089-2097. doi:10.1093/brain/awq122

Tavassoli, T., Latham, K., Bach, M., Dakin, S. C., & Baron-Cohen, S. (2011). Psychophysical measures of visual acuity in autism spectrum conditions. *Vision Res, 51*(15), 1778-1780. doi:10.1016/j.visres.2011.06.004

Tavassoli, T., Miller, L. J., Schoen, S. A., Nielsen, D. M., & Baron-Cohen, S. (2014). Sensory over-responsivity in adults with autism spectrum conditions. *Autism, 18*(4), 428-432. doi:10.1177/1362361313477246

Tomchek, S. D., & Dunn, W. (2007). Sensory processing in children with and without autism: a comparative study using the short sensory profile. *Am J Occup Ther, 61*(2), 190-200.

van der Geest, J. N., Kemner, C., Camfferman, G., Verbaten, M. N., & van Engeland, H. (2001). Eye movements, visual attention, and autism: a saccadic reaction time study using the gap and overlap paradigm. *Biol Psychiatry, 50*(8), 614-619.

Velmeshev, D., Schirmer, L., Jung, D., Haeussler, M., Perez, Y., Mayer, S., . . . Kriegstein, A. R. (2019). Single-cell genomics identifies cell type–specific molecular changes in autism. *Science, 364*(6441), 685-689. doi:10.1126/science.aav8130

Williams, B., Speed, A., & Haider, B. (2018). A novel device for real-time measurement and manipulation of licking behavior in head-fixed mice. *J Neurophysiol, 120*(6), 2975-2987. doi:10.1152/jn.00500.2018

Diminished cortical excitation during perceptual impairments in a mouse model of autism

Joseph Del Rosario, Anderson Speed, Hayley Arrowood, Cara Motz, Machelle Pardue, Bilal Haider

Supplementary figures

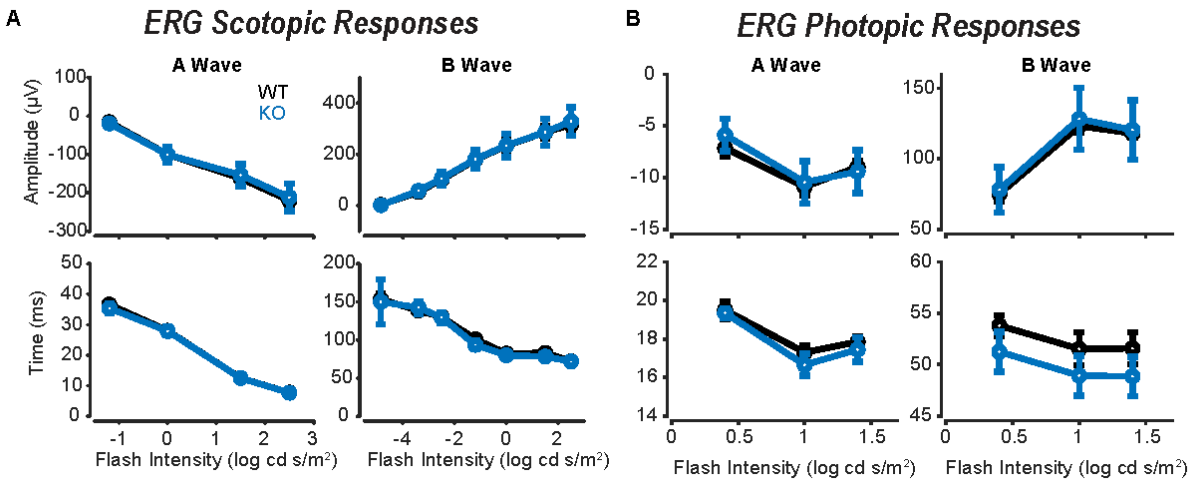

Figure 1–figure supplement 1. Retinal responses do not explain perceptual differences

a. Electroretinography (ERG) of scotopic responses (dark adapted; rod-dominated) as measured by the peak amplitude (top rows) and implicit time of the peak amplitude (bottom rows) for the initial negative deflection (a Wave, left) and the subsequent positive deflection (b Wave, right), which corresponds to the hyperpolarization of photoreceptor cells and depolarization of bipolar cells (Penn and Hagins, 1969). Neither the peak amplitude (a wave: *p=0.94*; b wave: *p=0.94*, n = 4 WT and 4 KO mice) nor implicit time (a wave: *p=1*; b wave: *p=0.52*) were significantly different between WT and KO mice. Mean ± SEM is plotted throughout the figure. See (Mees et al., 2019) for detailed description of ERG Methods.

b. Same as a, but for photopic responses (light adapted; cone-isolating). Neither the peak amplitude (a wave: *p=0.99*; b wave: *p=0.58*, 4 WT and 4 KO mice) nor implicit time (a wave: *p=0.62*; b wave: *p=0.08*) were significantly different between WT and KO mice.

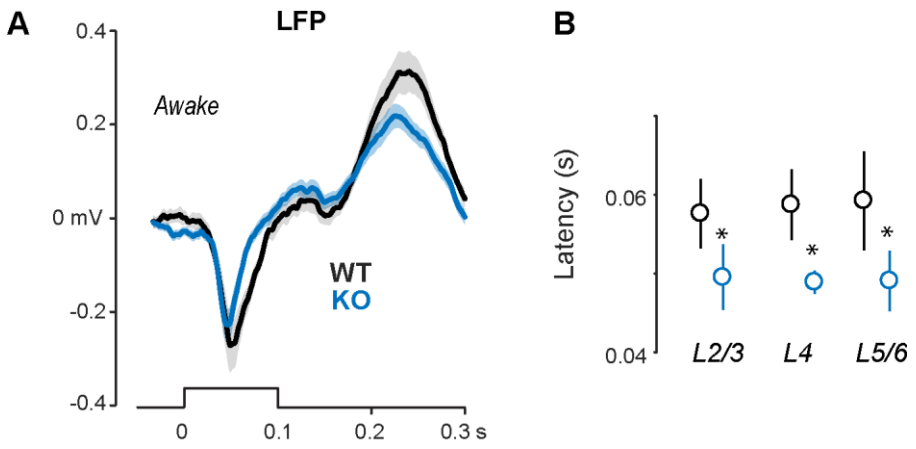

Figure 3–figure supplement 1. Laminar LFP response latencies across brain states in WT and KO mice

a. Population average LFP response across all layers to best bar (100% contrast, center of receptive field) for awake WT and KO mice. Mean ± SEM.

b. LFP response latency was significantly faster in KO mice across all layers.
L2/3: WT = 58 ± 42 ms, KO = 50 ± 4 ms (*p=0.05*, rank sum test).
L4: WT = 59 ± 4 ms, KO = 49 ± 1 ms (*p=0.01*, rank sum test).
L5/6: WT = 59 ± 6 ms, KO = 49 ± 4 ms (*p<0.01*, rank sum test).

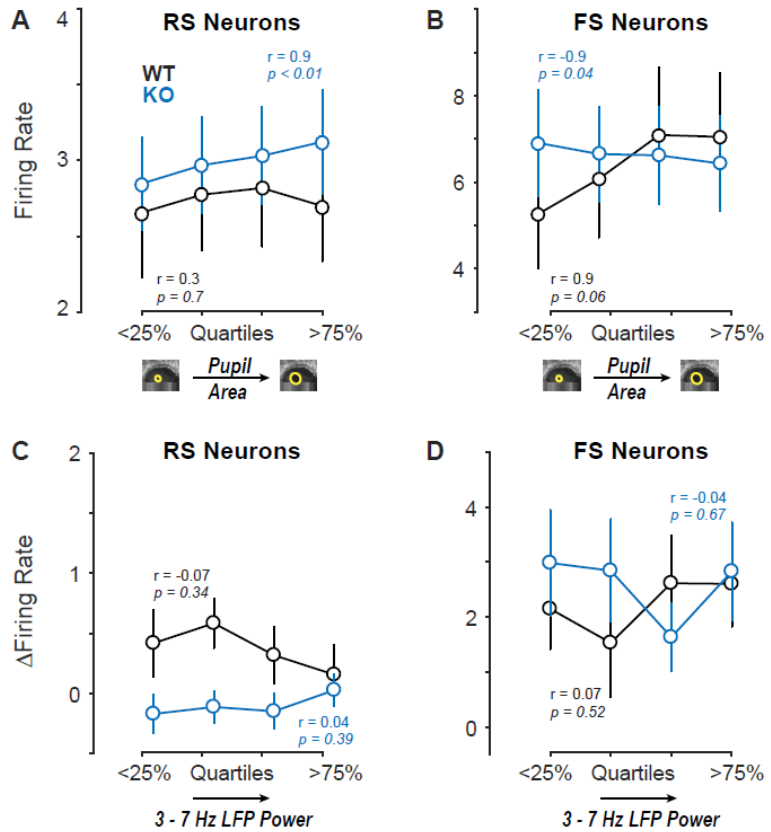

Figure 5–figure supplement 1. Firing rates in WT and KO mice as a function of pupil area and low frequency LFP power during behavioral task

- **a.** RS neuron firing rate preceding stimulus onset, sorted by single-trial pupil area quartile (relative to mean area overall during session mean area). Significant positive correlation of RS firing rate and pupil area in KO mice (r = 0.98, $p < 0.01$, n = 103 neurons, 1677 trials, 15 recordings in 3 mice) but not WT mice (r = 0.31, $p = 0.68$, n = 49 neurons, 744 trials, 7 recordings in 3 mice).
- **b.** Same as **a**, for FS neuron firing. Significant negative correlation of FS firing rate and pupil area in KO mice (r = -0.94, $p = 0.03$, n = 38 neurons, 1677 trials, 15 recordings in 3 mice) but not WT (r = 0.96, $p = 0.06$, n = 20, 744 trials, 7 recordings in 3 mice).
- **c.** Stimulus-evoked RS neuron firing rate (above baseline), sorted by 3 — 7 Hz LFP power quartiles. No significant correlation in KO (r = 0.04, $p = 0.39$, n = 103 neurons, 1677 trials, 15 recordings in 3 mice) or WT mice (r = -0.07, $p = 0.34$, n = 20, 744 trials, 7 recordings in 3 mice).
- **d.** Same as **c**,for FS neuron firing. No significant correlation in KO (r = -0.04, $p = 0.67$, n = 103 neurons, 1677 trials, 15 recordings in 3 mice) or WT mice (r = 0.07, $p = 0.52$, n = 20, 744 trials, 7 recordings in 3 mice).

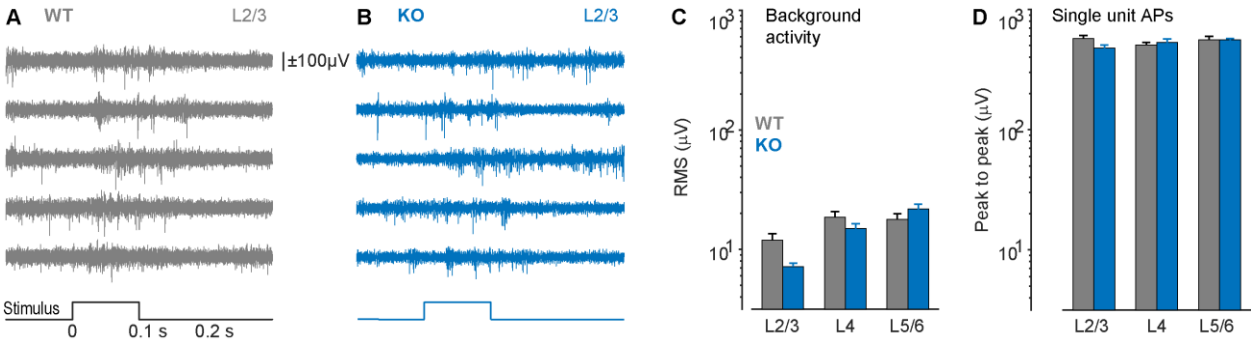

Figure 6–figure supplement 1. Background activity and spiking in WT and KO recordings

- **a.** Example single-trial raw signal (high pass >300Hz) from L2/3 in an awake WT mouse. 5 adjacent channels (25 micron spacing) show clear stimulus evoked spiking (bottom, 100% contrast flashed bar presented outside of behavioral task).
- **b.** Same as **a**, for L2/3 in awake KO mouse. Note that unresolved background activity ("hash") is not larger in KO recording versus WT recording.
- **c.** Root mean square (RMS) amplitude of background activity in L2/3 of KO mice is smaller than in WT mice (7 ± 1 μV vs 12 ± 2 μV, $p = 0.01$). No significant difference in other layers (L4: 15 ± 2 μV vs 19 ± 2 μV, $p = 0.14$; L5/6: 22 ± 2 μV vs 18 ± 2 μV, $p = 0.28$, *rank sum test*).
- **d.** Single unit AP amplitude was >1 order magnitude greater than background RMS noise in all layers of WT and KO mice. See also Fig. 6B.